Route to hyperbolic hyperchaos in a nonautonomous time-delay system

Cite as: Chaos **30**, 113113 (2020); https://doi.org/10.1063/5.0022645
Submitted: 22 July 2020 . Accepted: 05 October 2020 . Published Online: 05 November 2020

Pavel V. Kuptsov, and Sergey P. Kuznetsov

Chaos ARTICLE scitation.org/journal/cha

Route to hyperbolic hyperchaos in a nonautonomous time-delay system

Cite as: Chaos **30**, 113113 (2020); doi: 10.1063/5.0022645
Submitted: 22 July 2020 · Accepted: 5 October 2020 ·
Published Online: 5 November 2020

Pavel V. Kuptsov[1,2,3,a)] and Sergey P. Kuznetsov[3]

AFFILIATIONS

[1]Laboratory of Topological Methods in Dynamics, National Research University Higher School of Economics, Nizhny Novgorod, 25/12 Bolshay Pecherskaya St., Nizhny Novgorod 603155, Russia
[2]Institute of Electronic Engineering and Instrumentation, Yuri Gagarin State Technical University of Saratov, Politekhnicheskaya 77, Saratov 410054, Russia
[3]Kotel'nikov's Institute of Radio-Engineering and Electronics of RAS, Saratov Branch, Zelenaya 38, Saratov 410019, Russia

Note: This paper is part of the Focus Issue, Global Bifurcations, Chaos, and Hyperchaos: Theory and Applications.
[a)]**Author to whom correspondence should be addressed:** kupav@mail.ru

ABSTRACT

We consider a self-oscillator whose excitation parameter is varied. The frequency of the variation is much smaller than the natural frequency of the oscillator so that oscillations in the system are periodically excited and decayed. Also, a time delay is added such that when the oscillations start to grow at a new excitation stage, they are influenced via the delay line by the oscillations at the penultimate excitation stage. Due to nonlinearity, the seeding from the past arrives with a doubled phase so that the oscillation phase changes from stage to stage according to the chaotic Bernoulli-type map. As a result, the system operates as two coupled hyperbolic chaotic subsystems. Varying the relation between the delay time and the excitation period, we found a coupling strength between these subsystems as well as intensity of the phase doubling mechanism responsible for the hyperbolicity. Due to this, a transition from non-hyperbolic to hyperbolic hyperchaos occurs. The following steps of the transition scenario are revealed and analyzed: (a) an intermittency as an alternation of long staying near a fixed point at the origin and short chaotic bursts; (b) chaotic oscillations with frequent visits to the fixed point; (c) plain hyperchaos without hyperbolicity after termination visiting the fixed point; and (d) transformation of hyperchaos to the hyperbolic form.

A hyperchaotic attractor has at least two positive Lyapunov exponents, i.e., unlike a simple chaotic attractor, its phase space contains two or more expanding directions. In applications employing deterministic chaos, hyperchaotic systems are usually more preferable since their dynamics is more complicated in comparison with mere chaotic systems. However, many chaotic as well as hyperchaotic systems have actually a quasiattractor, i.e., a limit set containing stable periodic orbits, so that their dynamics is not so stochastic as expected. Good stochastic properties justified in a rigorous mathematical sense are guaranteed for the so-called hyperbolic attractors. Systems with attractors of this type demonstrate strong and structurally stable chaos that is insensitive to variation of functions and parameters in the dynamical equations, to noises, to interferences, etc. Our study in the present paper will be focused on a nonautonomous time-delay system with a hyperbolic hyperchaotic attractor. This system operates as two coupled hyperbolic chaotic subsystems. Varying its parameters, we can control the coupling strength between these subsystems as well as a mechanism responsible for their hyperbolic chaos. Due to this, a transition from non-hyperbolic to hyperbolic hyperchaos occurs. The following steps of the transition scenario are revealed and analyzed: (a) an intermittency as alternation of staying near a fixed point and chaotic bursts; (b) wandering between the fixed point and chaotic subset appears near it; (c) plain hyperchaos without hyperbolicity after termination visiting the fixed point; and (d) transformation of hyperchaos to hyperbolic form.

I. INTRODUCTION

Attractors characterized by two or more positive Lyapunov exponents are called hyperchaotic. The simplest and trivial example is provided by several chaotic systems with weak coupling whose

attractor is a direct sum of partial attractors.[1] However, the phase space dimension in this case is superfluous. The smallest possible dimension is four: two expanding directions, one contracting, and one neutral. The first nontrivial hyperchaotic attractor in a four-dimensional system was proposed by Rössler.[2]

Many studies were done around hyperchaotic dynamics since that time, and it still attracts the interest of researchers. In a recent paper,[3] routes of transition to hyperchaotic dynamics associated with different bifurcations of periodic and quasi-periodic regimes are revealed for coupled antiphase driven Toda oscillators. Garashchuk *et al.*[4] report a study of two coupled contrast agents being micrometer size gas bubbles encapsulated into a viscoelastic shell. Such bubbles are used for enhancing ultrasound visualization of blood flow and have other promising applications like targeted drug delivery and noninvasive therapy. For the onset of hyperchaotic dynamics in this system, a new bifurcation scenario is proposed that includes the appearance of a homoclinic chaotic attractor containing a saddle-focus periodic orbit with its two-dimensional unstable manifold. Moreover, it is shown that hypechaotic attractors are stable with respect to perturbations that destroy the synchronization manifold in the considered system. Radiophysical experiments with hyperchaotic dynamics as well as corresponding theoretical analysis are reported in Ref. 5. It is shown that as a result of a secondary Neimark–Sacker bifurcation, a hyperchaos with two positive Lyapunov exponents can occur in the system. A comparative analysis of chaotic attractors born as a result of the loss of smoothness of an invariant curve, period-doubling bifurcations, and secondary Neimark–Sacker bifurcation is carried out.

Hyperchaotic systems have more than one expanding direction in the phase space so that their dynamics is more complicated in comparison with mere chaotic systems. In particular, the prediction time of hyperchaotic regimes can be much less than that for chaos.[6] Thus, hyperchaotic oscillators are employed when the complexity of a signal is crucial, for example, for secure communications[7–10] and for image encryption.[11–14] One more promising application of hyperchaotic systems is damage assessment based on using a steady-state chaotic excitation.[15]

For applications where complexity is critical, one must take into account that many chaotic systems actually have a quasiattractor, i.e., a limit set containing stable periodic orbits, so the observable dynamics can be not so irregular as expected and be dramatically sensitive to small variations in parameters. Good scholastic properties justified in a rigorous mathematical sense are guaranteed for the so-called hyperbolic attractors. Systems with attractors of this type, like, for example, the Smale–Williams solenoid, demonstrate strong and structurally stable chaos that is insensitive to variation of functions and parameters in the dynamical equations, to noises, to interferences, etc.[16]

Hyperbolic attractors are composed exclusively of saddle trajectories.[17–19] For all their points, a space of small perturbations (tangent space) is split into a direct sum of subspaces that exponentially expand everywhere and contract. In the phase space, these subspaces are tangent to the corresponding expanding and contracting manifolds. In autonomous flow systems, in addition, there is a one-dimensional neutral tangent subspace of perturbations along a trajectory that corresponds to marginally stable shifts in time. A necessary and sufficient condition of the hyperbolicity is the absence of tangencies between stable, unstable, and neutral, if any, manifolds; only intersections at nonzero angles are admitted.

Due to their great potential importance for applications, structurally stable chaotic systems with hyperbolic attractors obviously have to be a subject of priority interest like rough systems with regular dynamics in the classic theory of oscillations.[20,21] However, for many years, hyperbolic attractors were commonly regarded only as purified abstract mathematical images of chaos rather than something intrinsic to real world systems. A certain progress in this field has been achieved recently when many examples of physically realizable systems with hyperbolic attractors have been purposefully constructed.[16,22]

A hyperchaotic system can be hyperbolic. An obvious example consists of two ordinary hyperbolic systems with weak coupling. Due to their structural stability, the hyperbolicity of the subsystems survives at least when the coupling is small so that the whole system is hyperbolic and hyperchaotic.

An interplay between hyperbolicity and hyperchaos was studied in Refs. 23 and 24. Kuptsov and Kuznetzov[23] report the scenario of transition to hyperchaos in a one-dimensional spatially distributed medium with local hyperbolic chaos. When its length is small, all spatial elements oscillate synchronously and demonstrate hyperbolic chaos. As the length grows, the second Lyapunov exponent becomes positive, and spatial homogeneity is destroyed. But, the hyperbolicity survives so that the system demonstrates a hyperbolic hyperchaos. Further growth of the length results in the emergence of the third positive Lyapunov exponent accompanied by violation of the hyperbolicity.

Kuptsov[24] considers the violation of hyperbolicity and transition to hyperchaos in a chain of diffusively coupled oscillators with hyperbolic chaos. It is shown that it occurs via an intermittency and so-called unstable dimension variability (UDV). The UDV regime is characterized by coexistence in the chaotic attractor of invariant periodic or chaotic orbits with different numbers of unstable directions.[25,26] Since trajectories of the system can pass close to these orbits, the dimensions of their unstable and stable manifolds vary. The UDV and intermittency as a part of scenario of transition to hyperchaos were also reported in Refs. 27–29. Other revealed details of the transition included a blowout bifurcation and bubbling.

Systems with a time-delay feedback combine simplicity of implementation and rich complexity of dynamics. Examples of such systems are wide-spread in electronics, laser physics, acoustics, and other fields.[30] Recently, several examples were suggested as physically realizable devices for the generation of rough hyperbolic chaos.[31–36] Though rigorous mathematical proof of their hyperbolicity is not performed yet, the hyperbolicity of these systems is confirmed numerically in Refs. 37 and 38.

Our study in the present paper will be focused on a nonautonomous time-delay system with a hyperbolic attractor suggested in Ref. 31. As discussed in Ref. 39, varying parameters of this system one can also obtain hyperbolic hyperchaotic attractors with as many positive Lyapunov exponents as required. In this paper, we study a hyperchaotic attractor with two positive Lyapunov exponents. We perform a numerical test that confirms its hyperbolicity and analyze the details of transition to hyperbolic hyperchaotic regime.

The paper is organized as follows. In Sec. II, we introduce a system and discuss how it operates. Also, we briefly review studying

methods that are used below. Section III discusses the transition from non-hyperbolic to hyperbolic hyperchaos. It is divided into several subsections: Subsection III A is focused on Lyapunov exponents, angle between expanding and contracting subspaces, and the Kaplan–Yorke dimension; Subsection III B represents two-dimensional distributions of various characteristic values on the attractor; in Subsection III C, we deal with the degenerated invariant subsets of the attractor; and Subsection III D discusses the large timescale behavior of finite time Lyapunov exponents (FTLEs). In Sec. IV, we outline the obtained results.

II. THE SYSTEM AND METHODS OF ANALYSIS

We will consider a nonautonomous system based on the van der Pol oscillator of natural frequency ω_0 supplied with a specially designed time-delay feedback,[31]

$$\ddot{x} - [A\cos(2\pi t/T) - x^2]\dot{x} + \omega_0^2 x = \epsilon x(t-\tau)\dot{x}(t-\tau)\cos\omega_0 t. \quad (1)$$

The parameter controlling the oscillator excitation is modulated with the period T and amplitude A. Modulation is slow, $T \gg 2\pi/\omega_0$, so that the positive half-period is sufficiently long for the periodic oscillations to grow up. Then, the oscillations decay and grow again at the next excitation stage corresponding to the next positive half-period of the modulation, see Fig. 1. The main harmonic at the nth excitation stage can be written as $\sin(\omega_0 t + \phi_n)$, where phase ϕ_n is controlled via the delay line. If the retarding time τ is close to $T/2$, as shown in Fig. 1(a), the emergence of the self-oscillations at each stage of activity is stimulated by a signal at the previous activity stage whose dominating harmonic is $\sin(\omega_0 t + \phi_{n-1})$. When it passes through a nonlinear delayed terms, the resonant harmonics $\sin(\omega_0 t + 2\phi_{n-1})$ with the doubled phase appears

$$\begin{aligned} &x(t-\tau)\dot{x}(t-\tau)\cos\omega_0 t \\ &\quad = \omega_0 \sin(\omega_0 t + \phi_{n-1})\cos(\omega_0 t + \phi_{n-1})\cos\omega_0 t \\ &\quad = (\omega_0/2)\sin(2\omega_0 t + 2\phi_{n-1})\cos\omega_0 t \\ &\quad = (\omega_0/4)\sin(\omega_0 t + 2\phi_{n-1}) + \ldots. \end{aligned} \quad (2)$$

This harmonic determines the phase ϕ_n of the new excitation stage when oscillations start to grow. To avoid its further influence and allow new oscillations to grow freely parameter, ϵ is taken small. As a result, we get a sequence of oscillation trains with phases at successive excitation stages obeying a chaotic Bernoulli-type map,

$$\phi_n = 2\phi_{n-1} + \text{const} \mod 2\pi. \quad (3)$$

(A constant addition appears since we transfer phase to the beginning of the stage and measure it in the middle.) According to argumentation in Ref. 31, this means that the attractor for the Poincaré map, which corresponds to states obtained stroboscopically at $t_n = nT$, is a Smale–Williams solenoid, and the respective chaotic dynamics is hyperbolic with the first Lyapunov exponent close to $\log 2$. In Ref. 37, this argumentation is confirmed via numerical test for τ values between approximately $T/4$ and $3T/4$.

The described mechanism of doubled phase transfer between excitation stages that results in hyperbolic chaos is reported for the first time in Ref. 40 and discussed in more detail in Refs. 16 and 22.

As reported in Ref. 39 using longer retarding times, say $\tau = 3T/2$ that provides the seeding of a new excitation stage from the stage before the previous one, see Fig. 1(b), it is possible to observe hyperchaos with two positive Lyapunov exponents. In this case, the map for phases at successive excitation stages looks as

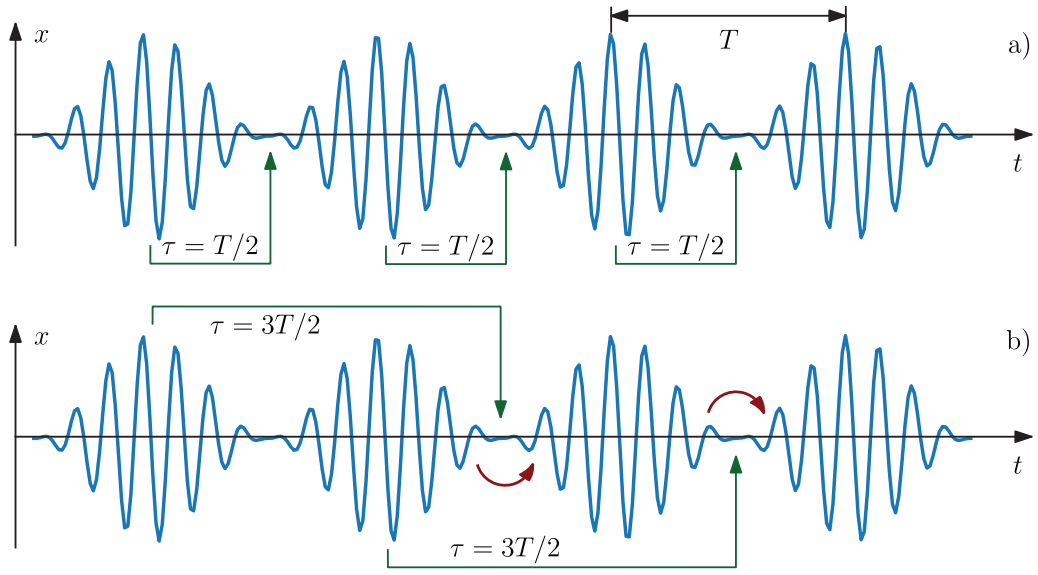

FIG. 1. Operation of system (1): (a) hyperbolic chaos and (b) hyperbolic hyperchaos with two positive Lyapunov exponents. Polyline arrows show the seeding transfer between excitation stages, and arc arrows show how the interaction between the subsystems occurs.

follows:

$$\phi_n = 2\phi_{n-2} + \text{const} \mod 2\pi. \tag{4}$$

The sequence of phases now contains two independent chaotic sequences whose elements alternate. Thus, system (1) in this case can be treated as consisting of two weakly coupled hyperbolic chaotic subsystems whose interaction produces hyperchaotic hyperbolic attractor. The subsystems interact on the boundary between excitations stages see the arc arrows in Fig. 1(b), and the hyperbolicity mechanism brings here the seeding with a doubled phase, see the polyline arrows. The type of dynamics depends on a relation between amplitudes of these two channels. This can be controlled by varying τ or T. If $\tau = 3T/2$, as in Fig. 1(b), then the hyperbolicity mechanism has the highest amplitude and, thus, dominates the coupling. In this case, the subsystems operate almost independently producing the hyperbolic hyperchaos. If $\tau \approx T$, then the hyperbolicity channel is the weakest so that the coupling prevails. In what follows, decreasing T, we will observe the transition to hyperbolic hyperchaos as a result of the decrease of the relative coupling strength.

In general, for

$$\tau = (k - 1/2)T, \quad k = 1, 2, 3 \ldots, \tag{5}$$

system (1) may be expected to have a hyperchaotic attractor with k positive Lyapunov exponents equal to $k^{-1} \log 2$.[39]

In this paper, we will focus on the case $k = 2$ for

$$\tau = 12,\ A = 3,\ \epsilon = 0.3,\ \omega_0 = 2\pi. \tag{6}$$

For sufficiently large modulation period, $T = 10$ dynamics of Eq. (1) is regular. When T gets smaller, hyperchaotic attractor appears, then it undergoes certain transformations and finally becomes hyperbolic. At $T = 8$, condition (5) is fulfilled exactly.

Due to the presence of the delay, system (1) is infinite-dimensional. Dealing with its computational model, we introduce discretization along time variable so that the dimension of the resulting model depends on the number of steps on the delay interval. Setting the step size $\Delta t = 0.01$ and taking the retarding time $\tau = 12$, we obtain for the second order delay differential equation (1), a numerical model whose phase space dimension is $N = 2402$.

We will analyze system (1) numerically using Lyapunov analysis. In brief, it includes studying of expanding and contracting properties of perturbation vectors and volumes spanned by these vectors as the system runs along a trajectory. The perturbation vectors are assumed to be infinitely small in magnitude and form a linear tangent space. The dimension of this space is equal to the phase space dimension N.

Globally, i.e., for an infinitely long trajectory, properties of the tangent vectors are described by a set of Lyapunov exponents λ_i, $i = 1, 2, \ldots N$, sorted in descending order. They can be treated in two ways. On the one hand, the sum of the first k Lyapunov exponents is an average rate of exponential expansion (or contraction, if negative) of every typical k-dimensional volume in the tangent space. On the other hand, the nth Lyapunov exponent is an average rate of exponential expansion of the nth covariant Lyapunov vector (CLV). These vectors are named "covariant" since nth vector at time t_1 is mapped by a tangent flow to the nth vector at time t_2 for any t_1 and t_2. There is a unique set of N such vectors. An arbitrary tangent vector does not have this property and merely converges to the first CLV. Two algorithms for computation of CLVs were first reported in the pioneering works.[41,42] See also Ref. 43 for more detailed explanation and discussion of one more algorithm. Also, see Ref. 44 for a survey.

Using the Lyapunov exponents, one can compute Kaplan–Yorke dimension of the attractor,[45]

$$D_{\text{KY}} = m + \frac{\sum_{i=1}^{m} \lambda_i}{|\lambda_{m+1}|}, \tag{7}$$

where m is such that $\sum_{i=1}^{m} \lambda_i > 0$ and $\sum_{i=1}^{m+1} \lambda_i < 0$. The Kaplan–Yorke dimension is related with the information dimension and is an upper estimate for the Hausdorff dimension of an attractor.[46]

The local structure of the attractor can be analyzed using finite time Lyapunov exponents (FTLEs) ℓ_i. There are two different sorts of these exponents. One is obtained in the course of the standard algorithm for Lyapunov exponents when we iterate a set of tangent vectors and periodically orthonormalize them using Gram–Schmidt or QR algorithms. Logarithms of their norms divided by the time step between the orthonormalizations may be called Gram–Schmidt FTLEs. This sort of FTLEs characterizes local volume expanding properties in the tangent space. The sum of the first k Gram–Schmidt FTLEs is a rate of local exponential expansion of a typical k-dimensional tangent volume. Their individual values except the first one have no much sense. Another sort of FTLEs are computed as local exponential expansion rates for CLVs. They characterize expansion or contraction for individual vectors in tangent space. In more detail, the difference between these two sorts of FTLEs is discussed in Ref. 47. In what follows, we will consider the CLV based FTLEs.

Dealing with FTLEs for flow systems, one have to choose an appropriate time step. This is not so obvious since the choice must be related somehow with intrinsic attractor time scales that are usually a priori unknown. One way to put the FTLEs analysis on the solid ground is to consider them on infinitesimally small times. Such instant FTLEs were introduced in Ref. 47. For discrete time systems, however, one can compute one step FTLEs. Since the system under consideration in this paper operates under external forcing with period T, it is natural to consider the corresponding stroboscopic map for it. Thus, all FTLEs below will be computed for one step of this map, i.e., for one period T in terms of the original flow system.

Another way of using FTLEs is to consider them on asymptotically long times. For large time scale, the Gram–Schmidt and the CLV based FTLEs coincide,[43] so it is reasonable to use the Gram–Schmidt ones since they require much less computational efforts. Due to the decay of correlations for a typical chaotic processes on large time scales, pairwise covariances of Lyapunov sums L_i (FTLEs not divided by time step) are expected to grow linearly. The matrix D_{ij} of the corresponding growth rates is introduced and studied in Ref. 48. Below, we analyze the covariances and show that for some parameter values they demonstrate power law instead of the expected linear growth.

To characterize the hyperbolicity, we will use the angle criterion. Chaotic attractor is called hyperbolic when all its trajectories

are of saddle type. It means that its expanding and contracting manifolds never have tangencies. Verification of this property can be done by checking the angles between tangent subspaces spanned by CLVs corresponding to positive and negative Lyapunov exponents (or, more rigorously, the smallest principal angle between these subspaces). The angle θ_i is the angle between a subspace spanned by the first i CLV and the subspace spanned by all the rest of them. If a discrete time system has k positive Lyapunov exponents and all others are negative, then it will be hyperbolic if θ_k never vanish along trajectories on the attractor. As we consider a system with two positive Lyapunov exponents, the indicating angle is θ_2. Notice that in actual computations starting from random initial conditions, we will never get exact zero angle. Instead, a typical trajectory can pass arbitrary close to points with zero angles. Thus, verifying the hyperbolicity, we can only check if the angles get very small. The fast method of computation of the angles is developed in Refs.[49] and 43. Its implementation for systems with a single time delay can be found in Ref. 37, and in Ref. 38, the generalization for the case of multiple delays is provided.

A chaotic attractor is known to contain invariant subsets, in particular, periodic orbits, and there are effective numerical methods for detection these embedded orbits.[50–52] Nevertheless, application of these methods for high-dimensional systems is rather problematic yet. In this paper, we develop another approach to detect some of the embedded invariant subsets.

Running along a trajectory we can encounter points where some of CLVs merge, i.e., the angle between them vanishes. It can occur either for vectors from unstable and stable subsets or for any other pair of vectors. Merging two CLVs means that the number of CLVs in this point is less by one compared to another attractor points. It means that we have here some degenerated invariant subsets. To provide a simple illustration assume that the attractor contains a fixed point with real eigenvalues. CLVs of this invariant subset are merely its eigenvectors. Let two eigenvalues coincide and the only one eigenvector corresponds to this degenerated pair (for example, this is always the case in two-dimensional space). Then, this will be exactly the situation described above. Thus, running along an attractor trajectory and collecting points where some of CLVs merge, we will detect degenerated invariant subsets embedded into the attractor.

The degenerated subsets can be identified by a signature constructed as a list of indexes of merging CLVs. Obviously, we cannot distinguish two subsets with identical signatures and they will be treated as a one subset. For each signature, we will compute CLV based FTLEs, i.e., average rates of exponential growths or decay of CLVs near the subsets. These partial FTLEs will be plotted against a control parameter to demonstrate how the subsets are transformed.

III. THE ANALYSIS

A. Lyapunov exponents, Kaplan–Yorke dimension, and angles between tangent subspaces

First, for system (1) with parameters (6), we consider a minimal angle, two Lyapunov exponents, and a Kaplan–Yorke dimension as functions of T decreasing from 10 to 7, see Fig. 2. Near $T = 10$, there are no positive Lyapunov exponents, as one can see in Fig. 2(a). It corresponds to regular oscillations in the system.

Transition to chaos and then to hyperchaos is illustrated in Fig. 3 where the enlarged area of Fig. 2(a) is shown. One can see that the dynamics becomes chaotic at approximately $T = 9.835$. There is a very narrow area where only one Lyapunov exponent is positive, and very soon approximately at $T = 9.8$, the second one also becomes positive, so the hyperchaotic regime appears. Observe very small slope of the curve λ_2: it goes almost horizontally when passes zero. This is typical behavior for transition to hyperchaos

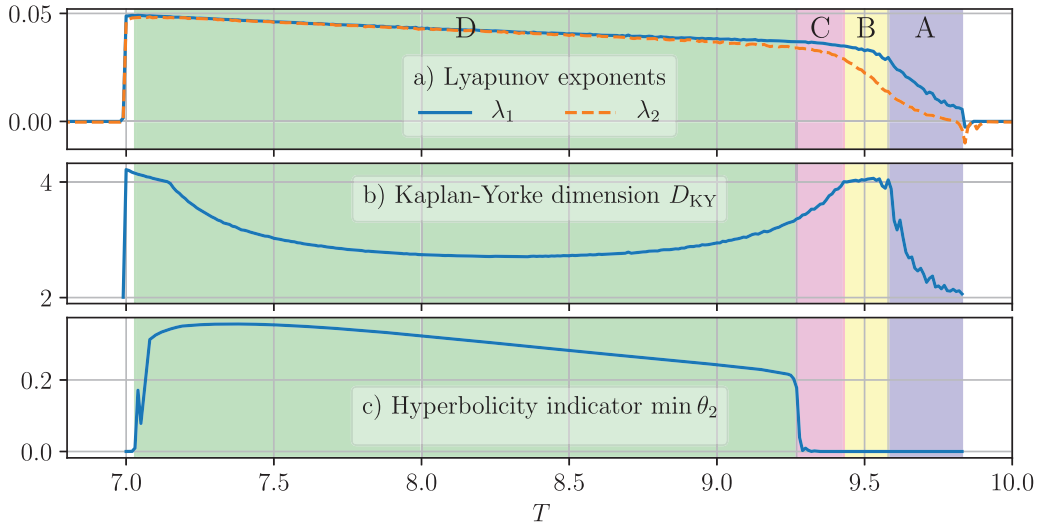

FIG. 2. (a) Lyapunov exponents, (b) Kaplan–Yorke dimension, and (c) minimal angle θ_2 between expanding and contracting tangent subspaces. Shaded areas A–D highlight ranges of different attractor types.

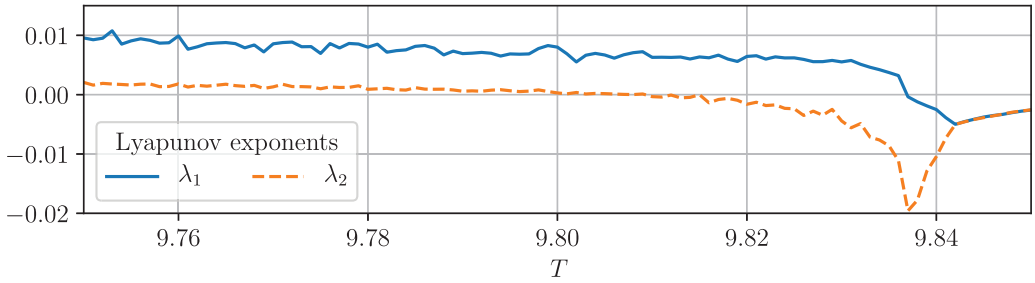

FIG. 3. Enlarged area of Fig. 2(a) where the transition from chaos to hyperchaos occurs.

owing to the bifurcations of unstable periodic orbits embedded into attractor.[28] In our case, the area where λ_2 stays close to zero is very narrow.

The parameter interval of our interest can be split into four areas that we mark by capital letters A, B, C, and D, see Fig. 2. Area A starts when the system becomes hyperchaotic at $T = 9.8$ and extends to $T = 9.58$ until the Kaplan–Yorke dimension grows, see Fig. 2(b). The minimal angle $\min\theta_2$ between the expanding and contracting subspaces remains close to zero [see Fig. 2(c)] indicating non-hyperbolicity of chaos within this area. Area B covers the range where the Kaplan–Yorke dimension is constant and ends at approximately $T = 9.43$. The minimal angle $\min\theta_2$ is still zero, i.e., chaos is non-hyperbolic. Area C stretches up to a point of transition to hyperbolic chaos, i.e., to a point where the minimal angle θ_2 starts to grow. It occurs at approximately $T = 9.27$. Finally, area D corresponds to hyperbolic hyperchaos with two positive Lyapunov exponents. At the boundary of this area, first two Lyapunov exponents approach each other and merge, see Fig. 2(a). As discussed above, the considered system operates as two identical alternating chaotic subsystems. The value of T controls their relative coupling strength with respect to the phase doubling mechanism responsible for the hyperbolicity, see Fig. 1(b), and the related discussion. Thus, the hyperbolic hyperchaos in our system emerges when the coupling strength between the subsystems becomes sufficiently weak so that they demonstrate almost identical dynamics. The area of hyperbolic hyperchaos ends at approximately $T = 7.02$. Beyond this point, the system remains hyperchaotic within the very narrow interval and then oscillations become regular.

B. Probability density functions on the attractor

To examine the attractor structure in areas A–D, we will consider now probability density functions (PDFs) of dynamical variables and related characteristic values, see Fig. 4. Plots in this figure are grouped in five columns. The first three of them, from (a) to (c), correspond to the areas from A to C in Fig. 2, and two last columns (d) and (e) represent area D. Column (d) characterizes a hyperchaotic hyperbolic attractor close to the transition point and (e) corresponds to the case when relation (5) is fulfilled exactly for $k = 2$, i.e., $\tau = 1.5T$. All plots are computed for the stroboscopic map at $t = nT$.

1. Area A

Figure 4($a_{1,2,3,4}$) is plotted at $T = 9.7$ that corresponds to area A. Panel (a_1) shows PDF of x and $\dot{x}/\omega_0$. Since the phase space dimension is high, these plots can be considered as two-dimensional projections of multidimensional PDFs. Observe a sharp spike at the origin visible as a dark spot. The spot is surrounded by a wide pale area representing wandering of the system in the vicinity of the origin.

The observed structure of the PDF is caused by intermittency, see Fig. 5(a). In this figure, we plot the phase space distance of the orbit to the origin

$$\rho(t) = \sqrt{x(t)^2 + (\dot{x}(t)/\omega_0)^2} \tag{8}$$

for time sliced stroboscopically at $t = nT$. One can see alternation of laminar phases when the system is close to zero with burst of oscillations. Figure 6 provides further confirmation of the intermittent nature of the considered regime. It shows a distribution of lengths of laminar trajectory cuts when the phase space trajectory is near the origin. Here and below, power law distributions as well as estimation of the exponent α is done with the help of Python package "powerlaw."[53] In the log–log scale, the distribution admits linear approximation that corresponds to the power law. The computed exponent is $\alpha = -1.95$.

Figure 4(a_2) shows the PDF of ρ and maximal FTLE $\max\ell_i$, $i = 1, 2, \ldots$. Here and below, FTLEs ℓ_i are computed as average exponential growth rates of CLVs over time T, corresponding to one step of the stroboscopic map. Since FTLEs strongly fluctuate, they are usually not ordered in the descent order in contrast to the global Lyapunov exponents. Hence, on each step, we simply take the largest one.

The PDF of ρ and $\max\ell$ in Fig. 4(a_2) shows locations of areas of chaotic divergence on the attractor and areas where close trajectories approach each other. One can see a spike at $\rho = \max\ell = 0$. It corresponds to the laminar phases and indicates that near the origin, the trajectories basically demonstrate marginal stability. To explain this, we need to take into account that $x = \dot{x} = 0$ is a fixed point for considered system (1). Linearization near this point results in a linear equation with parametric excitation with period T. Since the excitation parameter oscillates symmetrically near zero, on average, the fixed point at the origin is marginally stable.

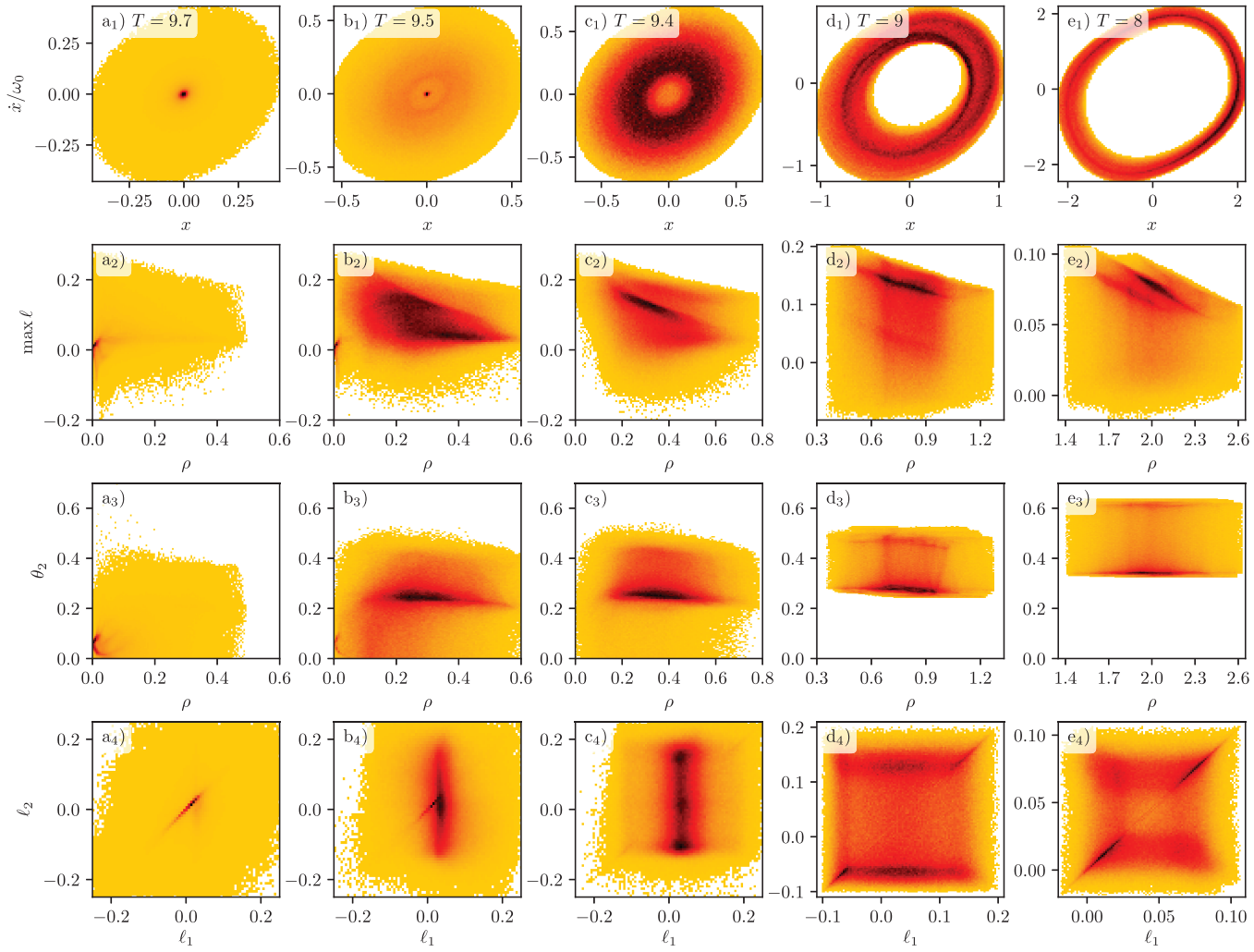

FIG. 4. Numerical approximations of probability density functions (2D histograms) on the attractor. Columns (a), (b), and (c) correspond to areas A, B, and C in Fig. 2, respectively, and columns (d) and (e) correspond to area D. Values of T are given in the legends on the top row and are the same along the columns. Values on the vertical axis in the leftmost column are the same along rows. Darker areas represent higher densities.

Figure 4(a_3) shows the PDF of ρ and the angle θ_2 whose zero indicates a tangency between expanding and contracting manifolds, i.e., reveals points of the hyperbolicity violation. From Fig. 2(c), we know that within the area A chaos is non-hyperbolic. And from Fig. 4(a_3), we see that the violation of the hyperbolicity preferably occurs near the origin: one can see the spike near $\rho = 0$ where θ_2 often vanishes. Beyond the origin, the vanishing angles are more rare.

Figure 4(a_4) represents the PDF of the first two FTLEs ℓ_1 and ℓ_2. The dark line along the diagonal near the origin corresponds to equal ℓ_1 and ℓ_2. Identical Lyapunov exponents reflect a symmetry of dynamics with respect to some variables interchange. As discussed above, see Fig. 1, within the considered parameter range, the system can be treated as two weakly coupled chaotic subsystems. The stripe along the diagonal in Fig. 4(a_4) indicates that these two subsystems behave coherently, i.e., synchronized, when pass the origin.

2. Area B

The PDF of x and $\dot{x}/\omega_0$ in area B, see Fig. 4(b_1), looks very similar to the previous case in Fig. 4(a_1). The only difference is a barely visible darker area surrounding the origin. But actually, it indicates a qualitative change of the behavior. One can see in Fig. 5(b) that though a trajectory still often visits the origin neighborhoods, this is not an intermittency.

The PDF of ρ and $\max \ell$ in Fig. 4(b_2) reveals the emergence in area B of a new structure. Like in area A, see Fig. 4(a_2), we observe the spike at $\rho = \max \ell = 0$ corresponding to the passing of

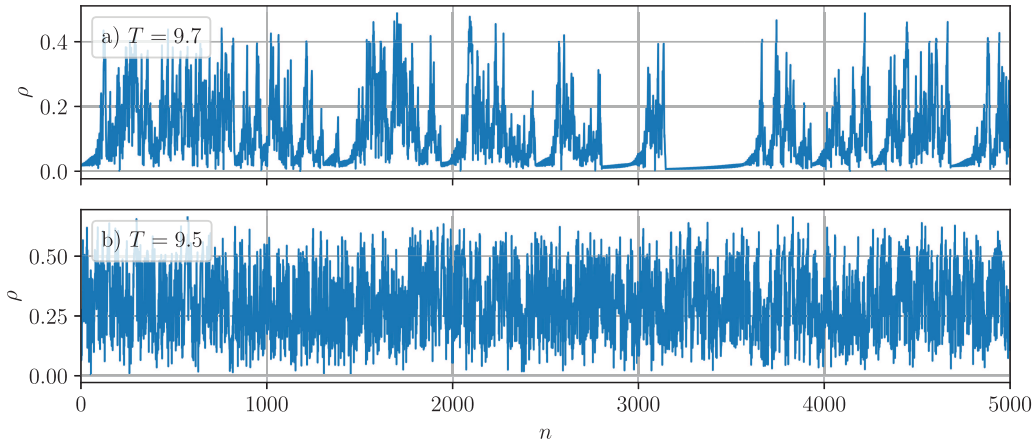

FIG. 5. Time series of distances to the origin for (a) $T = 9.7$, area A and (b) $T = 9.5$, area B.

a trajectory near the fixed point at the origin. But also, a massive bulk of points appears at positive max ℓ and nonzero ρ. It represents a chaotic subset embedded into the attractor. Thus, in area B, the dynamics is determined by a wandering of the system between this chaotic subset and the fixed point at the origin.

The PDF of ρ and θ_2 in Fig. 4(b_3) again, similarly to the area A, see Fig. 4(a_3), contains the spike near $\rho = \theta_2 = 0$ (now barely visible due to the presence of another maxima) but also a large spot corresponding to a new chaotic subset. Most of points within this spot are hyperbolic, i.e., located at $\theta_2 > 0.2$. However, their noticeable number is characterized by a vanishing angle: observe getting down to $\theta_2 = 0$ darker arm centered at approximately $\rho = 0.2$.

The PDF of ℓ_1 and ℓ_2, see Fig. 4(b_4), again contains the diagonal line near zero mentioned already in area A in Fig. 4(a_4) and corresponding to the coherence of the subsystems near the origin. Also, a very well pronounced is the vertical stripe representing strong fluctuation of the second FTLE ℓ_2. The first one ℓ_1, on contrary, is well localized.

Altogether, in area B, a new embedded non-hyperbolic chaotic subset emerges but the fixed point at the origin is essential yet and trajectories wander between these two subsets. Due to this wandering, the FTLEs ℓ_1 and ℓ_2 switch between coherency at the origin and strong fluctuation of ℓ_2 at the chaotic subset. As shown below, the

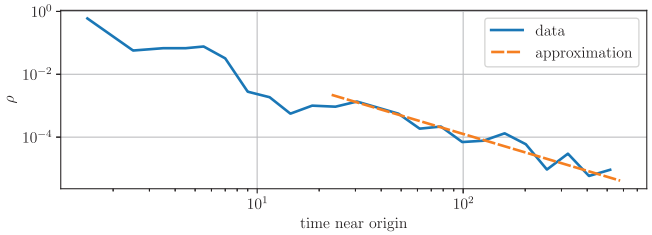

FIG. 6. Distribution of laminar phases $\rho < 0.05$ and its power law approximation with the exponent $\alpha = 1.95$ that corresponds to Figs. 4(a) and 5(a), area A.

presence of two competing embedded subsets results in anomalous diffusion of Lyapunov exponents.

3. Area C

Figure 4(c_1) corresponds to area C. One can see that a darker and barely visible circular structure in Fig. 4(b_1) is now turned into a well formed ring where trajectories spend most of time. There is no maximum corresponding to the fixed point at the origin anymore but its neighborhood is still visited.

In Fig. 4(c_2), we observe that the spike at $\rho = \max \ell = 0$ disappears at all, and the origin $\rho = 0$ is characterized by a positive FTLE. Thus, the chaotic subset first appeared in Fig. 4(b_2) now dominates. Representing it structure on the PDF becomes sharper in comparison with Fig. 4(b_2): one can see well defined dark stripe on the plot indicating that the most probable largest FTLEs decrease as ρ grows.

Figure 4(c_3) also confirms disappearance of the structure representing the fixed point at the origin. The dominating chaotic subset becomes "more hyperbolic" insofar as the getting down arm near $\rho = 0.2$ disappears and less number of points has the vanishing angle θ_2.

In accordance with the changed role of the fixed point, in Fig. 4(c_4), no diagonal stripe is visible representing the coherence of ℓ_1 and ℓ_2 at the origin. The only most visited structure is a vertical stripe corresponding to the chaotic subset that now dominates. Moreover, barely visible are two more features. The first is a pair of diagonal segments appeared beyond the origin at approximately $\ell_1 = \ell_2 \approx \pm 0.15$, and the second are darker areas to the left and to the right from the main vertical stripe representing a more intense fluctuations of ℓ_1. These features are precursors of a hyperchaotic hyperbolic attractor that appears in the course of further decrease of T.

4. Area D

Figures 4(d) and 4(e) represent a hyperchaotic hyperbolic attractor, area D in Fig. 2. The common feature is that trajectories never visit vicinities of the origin, see Figs. 4(d_1) and 4(e_1). It means

that the oscillation phase that is responsible for the hyperbolic chaos is now well defined.[39]

Inspection of PDFs in Figs. 4(d_1) and 4(e_1) reveals two different forms of the attractor. At $T = 9$, i.e., just after the transition to the hyperbolicity, there are two loops formed by the most visited points while far from the transition at $T = 8$, only one main loop is visible. We recall that hyperchaos in considered system (1) is the result of interaction of two coupled chaotic subsystems, see Fig. 1(b) and the related discussion. When T is decreased, the coupling strength between the subsystems becomes weaker while the hyperbolicity mechanism, related with the phase doubling, becomes stronger. Comparing Figs. 4(d_1) and 4(e_1), we can see that it results in more coherent behavior of these subsystems that manifests itself as a merge of the two loops.

Visually, the attractor in Fig. 4(d_1) looks more complicated than the attractor in Fig. 4(e_1), and one can expect that its dimension is higher. This intuition agrees with Fig. 4(b): the Kaplan–Yorke dimension decreases as T is varied within area D from $T = 9$ to $T = 8$.

PDF of ρ and $\max \ell$ has a single stripe when the coupling between the chaotic subsystems is stronger at $T = 9$, see Fig. 4(d_2) while weaker coupling at $T = 8$ results in two parallel stripes. The latter indicates that two chaotic subsets may be distinguished in the phase space, and a trajectory wanders between them. Taking into account the discussion of Figs. 4(d_1) and 4(e_1) that at $T = 8$, the two subsystems are more coherent, one can assume that these subsets correspond to synchronized and non-synchronized segments of trajectories. Unlike the case in Fig. 4(b_2), these two subsets have similar properties so that, as we will discuss below, their presence does not affect the normal convergence of Lyapunov exponents. Also, notice that most of points in Figs. 4(d_2) and 4(e_2) are located at positive values of $\max \ell$. It means that already locally the fluctuations of FTLEs are sufficiently weak.

Also, the emergence of the two subsets at $T = 8$ is visible in the PDFs of ρ and θ_2, see Figs. 4(d_3) and 4(e_3). In panel d_3, we observe the main dominating structure as a dark horizontal stripe at the bottom of the plot, while in panel (e_3), one also can see one more horizontal stripe at the top part. It means that the two chaotic subsets has different distributions of angles between expanding and contracting manifolds though in both cases the angles are non-vanishing. The latter again confirms the hyperbolicity of chaos in area D.

In the PDF for ℓ_1 and ℓ_2 in Fig. 4(d_4), the features barely visible in Fig. 4(c_4) are well pronounced. Both FTLEs fluctuate with almost identical amplitudes. Both positive and negative values are encountered but the fluctuations are strongly biased to the positive side. Prevailing structures are two horizontal stripes representing fluctuations of ℓ_1 and two short diagonal segments corresponding to synchronous oscillations of the two subsystems. Since the presence of the synchronized segments is revealed only in PDF of ℓ_1 and ℓ_2, we conclude that at $T = 9$, the coherency between the subsystems occurs but it is week and seldom.

As T is decreased up to 8, the PDFs of ℓ_1 and ℓ_2 become symmetric with respect to the main diagonal, see Fig. 4(e_4). It demonstrates the presence of two identical chaotic subsystems that can oscillate coherently, see the well formed diagonal stripe. But they do not stay synchronized for all time. Ends of the coherent stages associated with leaving the symmetric attractor are represented by symmetric off diagonal structures. Also, notice that the whole area of FTLEs fluctuations is roughly four times narrower than in the previous cases and fluctuating FTLEs are preferably positive.

C. Degenerated invariant subsets

When we move along an attractor trajectory and compute CLVs γ_i, we can register cases when some of the vectors merge. This happens when we pass close to a degenerated invariant subset with smaller number of independent CLVs. Such subsets can be identified by signatures of the form $\gamma_i = \gamma_j$, indicating what vectors coincide, and characterized by partial Lyapunov exponents $\lambda^{(\mathrm{part})}$ computed as averages of the corresponding FTLEs near these subsets.

1. Partial Lyapunov exponents for the degenerated subsets

Figure 7 represents partial Lyapunov exponents (left column) and their percentage (right column) for the degenerated subsets. The latter refers to a number n of encountered points with a certain signature divided by the total number of the checked attractor points $N = 10^6$ and multiplied by 100. We show signatures with noticeable percentages only. Those with $n \leq 50$ are omitted.

Figure 7(a) represent trajectory points without peculiarities, i.e., those where no merging of CLVs occurs. As one can see in panel (a_2) that their percentage is close to 100 so that the curves in Fig. 7(a_1) almost coincide with the ordinary global Lyapunov exponents, cf. Fig. 2(a).

Figures 7(b)–7(d) demonstrate the largest degenerated subsets. Their signatures are $\gamma_1 = \gamma_2$, $\gamma_3 = \gamma_4$, and $\gamma_5 = \gamma_6$, respectively. Their percentages are around $0.1 \div 0.2$, see panels (b_2)–(d_2). Observe that partial Lyapunov exponents in the panels (b_1)–(d_1) are similar to those without merging CLVs in Fig. 7(a_1). The common feature of these three cases is that the exponents are either pairwise coincide or close to each other: 1 and 2, 3 and 4, and 5 and 6. This is the manifestation of the presence of two chaotic subsystems, see Fig. 1(b) and the related discussion. Pairwise closeness of the exponents is related with the coherence of these subsystems, discussed above.

The percentage of the subset $\gamma_2 = \gamma_3$ in Fig. 7(e) is smaller in order of magnitude. However, this subset is nevertheless essential. We recall that the whole attractor has two-dimensional expanding manifold so that the vanishing angle between the second and the third CLVs indicates the destruction of the hyperbolicity. Thus, Fig. 7(e_1) represents the subset responsible for the violation of the hyperbolicity. Observe that it disappears in the middle of area C, before the expected transition to hyperbolicity on the C–D boundary. This is explained in Fig. 7(e_2). One can see that the number of the encountered points monotonically decays within the area C as T approaches area D. The system visits the subset $\gamma_2 = \gamma_3$ more and more seldom so that one have to trace longer and longer trajectories to detect this subset close to the transition point.

Also, notice that the destructing hyperbolicity subset $\gamma_2 = \gamma_3$ has the largest percentage in area A. This agrees well with the previous observations in Figs. 4(a_3)–4(e_3): the highest maximum of

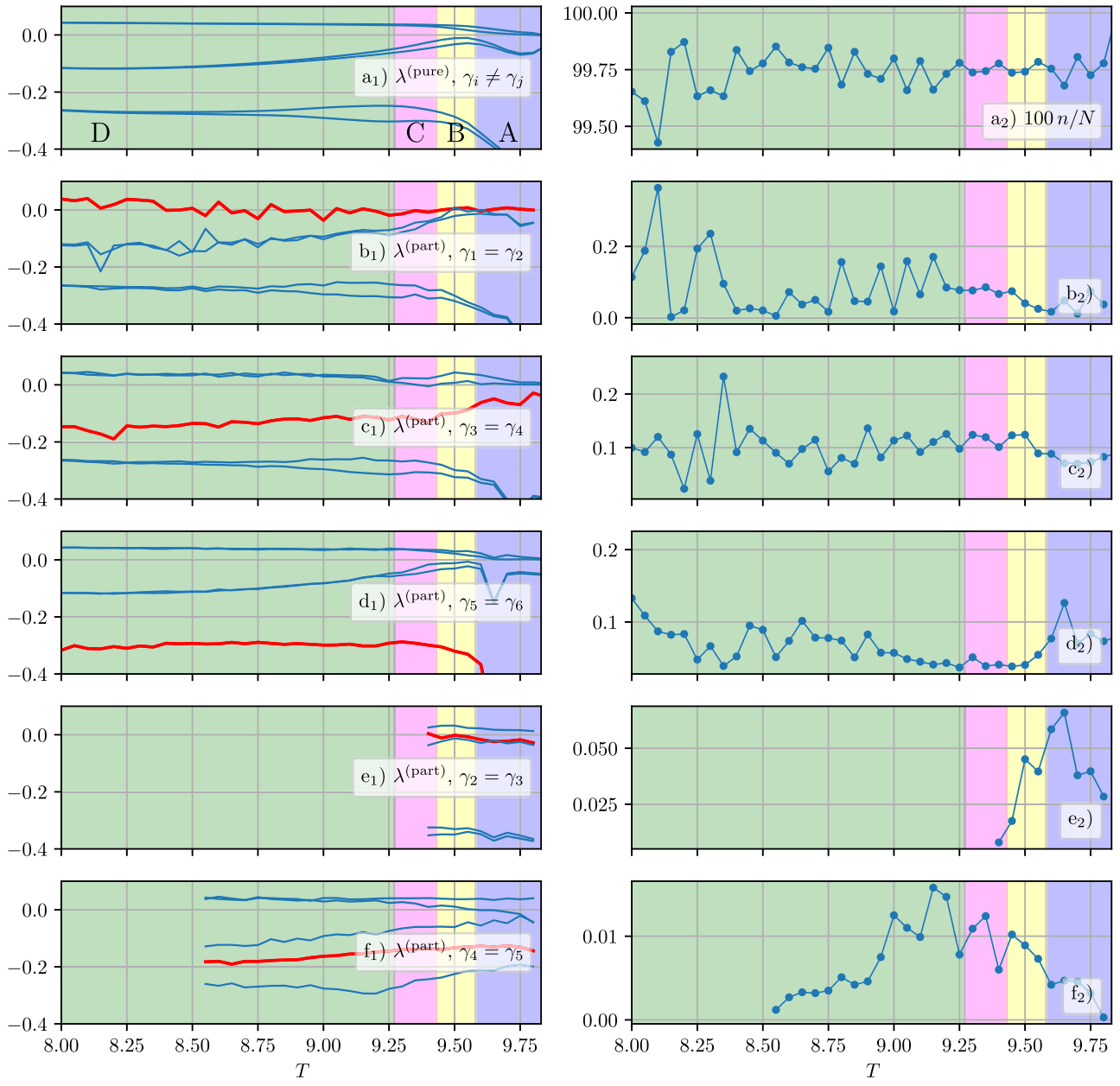

FIG. 7. Left panel (a_1): Lyapunov exponents computed for trajectory points where no CLV coincide. Other panels below it: partial Lyapunov exponents computed for degenerated invariant subsets where some of CLVs coincide, see panel legends. Fat red lines highlight the identical partial Lyapunov exponents corresponding to the merged CLVs. Right panel (a_2) and the panels below: relative size 100 n/N of the subset for that the corresponding left panel is plotted. Here, $N = 10^6$ is the total trajectory length, and n is the number of encountered subset points.

PDF near $\theta_2 = 0$ indicating the disappearance of the hyperbolicity is observed in the area of intermittency A.

The percentage of the subset $\gamma_4 = \gamma_5$ in Fig. 7(f) is also relatively small. This subset becomes hyperchaotic in area B, and two largest Lyapunov exponents become almost identical in area D, when the whole system becomes hyperbolic. Since its second and third CLVs do not merge, this subset is hyperbolic. Also, it is located far from the symmetric manifold where the two subsystems are synchronized since their partial Lyapunov exponents are not close pairwise as in Figs. 7(b)–7(d). It explains the existence of two

forms of hyperbolic attractors that where demonstrated in Figs. 4(d) and 4(e): less coherent attractor [column (d)] exists to the right of $T \approx 8.5$ when the subset in Figs. 7(f) is visited, and it becomes more coherent [column (e)] when this subset disappears.

2. Bias of global Lyapunov exponents due to the degenerated subsets

Now, we estimate the overall influence of the degenerated subsets. For each T, we first compute Lyapunov exponents λ_i as average of all CLV FTLE encountered along a trajectory. Then, we compute purified Lyapunov exponents $\lambda_i^{(\text{pure})}$ ignoring those FTLEs obtained at points near the degenerated subsets. Finally, we estimate the relative bias introduced by the subsets as

$$\delta\lambda_i = \left| \frac{\lambda_i - \lambda_i^{(\text{pure})}}{\lambda_i} \right|. \tag{9}$$

Figure 8 shows the maximal relative bias computed for six Lyapunov exponents as $\max\{\delta\lambda_i | i = 1, 2, \ldots, 6\}$. Observe clear difference of areas A–D. In area A, where the system demonstrates intermittency, the bias is the highest. Area B is characterized by the presence of two competing subsets embedded into the attractor. In the beginning of this area, the bias first drops down but then grows again. In area C, where the system has chaotic non-hyperbolic attractor, the bias remains at a constant level.

In area D, where the attractor becomes hyperbolic, we observe a decrease of the bias. It occurs until the subset $\gamma_4 = \gamma_5$ is visited, see Fig. 7(f) so that the hyperbolic attractor has the less coherent form shown in Fig. 4(d). After the disappearance of this subset, when the attractor becomes more coherent [see Fig. 4(e)], the bias stays at more or less constant small level. Small bias due to the degenerated subsets is related with structural stability and uniformity of the hyperbolic attractor, see Refs. 16 and 22 for the discussion of these concepts.

D. Large time FTLEs

Another approach considers fluctuations of FTLEs on large times. Large time FTLEs averaged over $\Delta t = \theta T$ time intervals will be denoted as $\mathscr{L}_i$.

When oscillations are chaotic or hyperchaotic, computing large time FTLEs, we deal with sums of nearly independent random values.[48,54] It means that PDF of large time FTLEs is expected to be Gaussian, and the summation can be treated as a diffusion process with linear growth of dispersion.[48,54] When this is indeed the case, the diffusion of Lyapunov exponents is said to be normal. Otherwise, it is anomalous. Below, we will see that the considered system can demonstrate behaviors of both types.

1. Distributions of large time FTLE

Figure 9 shows PDFs for the first large time FTLE computed at $\theta = 256$, 1024, and 4096. The left column represents $\mathscr{L}_1$ itself and the right one is for absolute values of deviations of $\mathscr{L}_1$ from the mean $\langle \mathscr{L}_1 \rangle = \lambda_1$. In the right column, the logarithmic scale is used on the vertical axis.

Figure 9(a) corresponds to area A, where the system demonstrates intermittency and laminar phases obeys power law, see Fig. 6. Hence, laminar phases of arbitrary lengths can appear with a nonzero probability, and small $\mathscr{L}_1$ can be encountered regardless of θ. As a result, the corresponding PDF of $\mathscr{L}_1$ always has a nonzero but asymptotically decaying peak at the origin. This is illustrated in Fig. 9(a_1). One can see that this peak is very high at $\theta = 256$, and it is still visible at $\theta = 1024$. The left tail of the PDF at $\theta = 4096$ does not reach the origin but this is because the number of points accumulated for computation of PDF is not enough to take into account very long laminar phases.

If we ignore the left end of the curve, the rest looks Gaussian. The main its feature, the exponentially decaying tails, is confirmed in Fig. 9(a_2). One can see here that in the logarithmic scale on the vertical axis, the tails of PDFs at $\theta = 1024$ and $\theta = 4096$ decay linearly that corresponds to the exponential law. This Gaussian form correlates with the uniform distribution of the one step FTLE ℓ_1 outside of the origin, see Fig. 4(a_4).

In area B, there are two competing structures in the phase space: one is the fixed point at the origin and the other is a chaotic subset, see Fig. 4(b_2). Their stability properties are strongly different. Wandering between them results in non-Gaussian distributions of FTLEs. One can see in Fig. 9(b_1) that regardless of the averaging time there is an essential tail spreading to the origin. This tail is also shown in Fig. 9(b_2). One can see here that the deviations decay is essentially slower than the exponent. To further characterize PDF in this case, we re-plot it in Fig. 9(b_2) in the log–log scale, see Fig. 10. Linear decay of the tails indicate power law distribution, known as distribution with heavy tails. The exponents of this distribution α are given in Fig. 10. One can see that it approaches to 3 as θ grows.

The PDFs in areas C (non-hyperbolic chaos) and D (hyperbolic chaos) demonstrate plain behaviors, typical for common chaotic dynamics. The curves are Gaussian, see Figs. 9(c_1) and 9(d_1), and their tails decay exponentially, see Figs. 9(c_2) and 9(d_2). Notice that this is observed regardless of the presence of the hyperbolicity: the

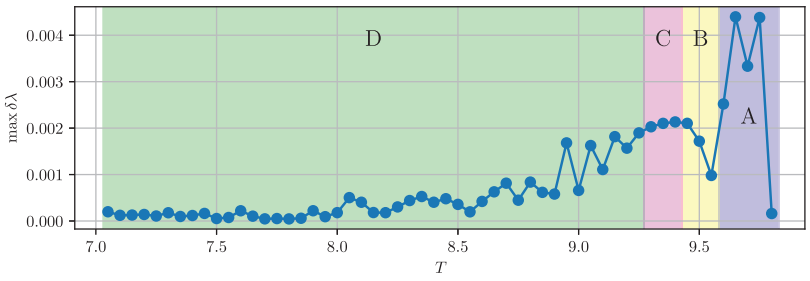

FIG. 8. Maximal relative bias of Lyapunov exponents due to the degenerated subsets $\max\{\delta\lambda_i | i = 1, 2, \ldots, 6\}$, see Eq. (9).

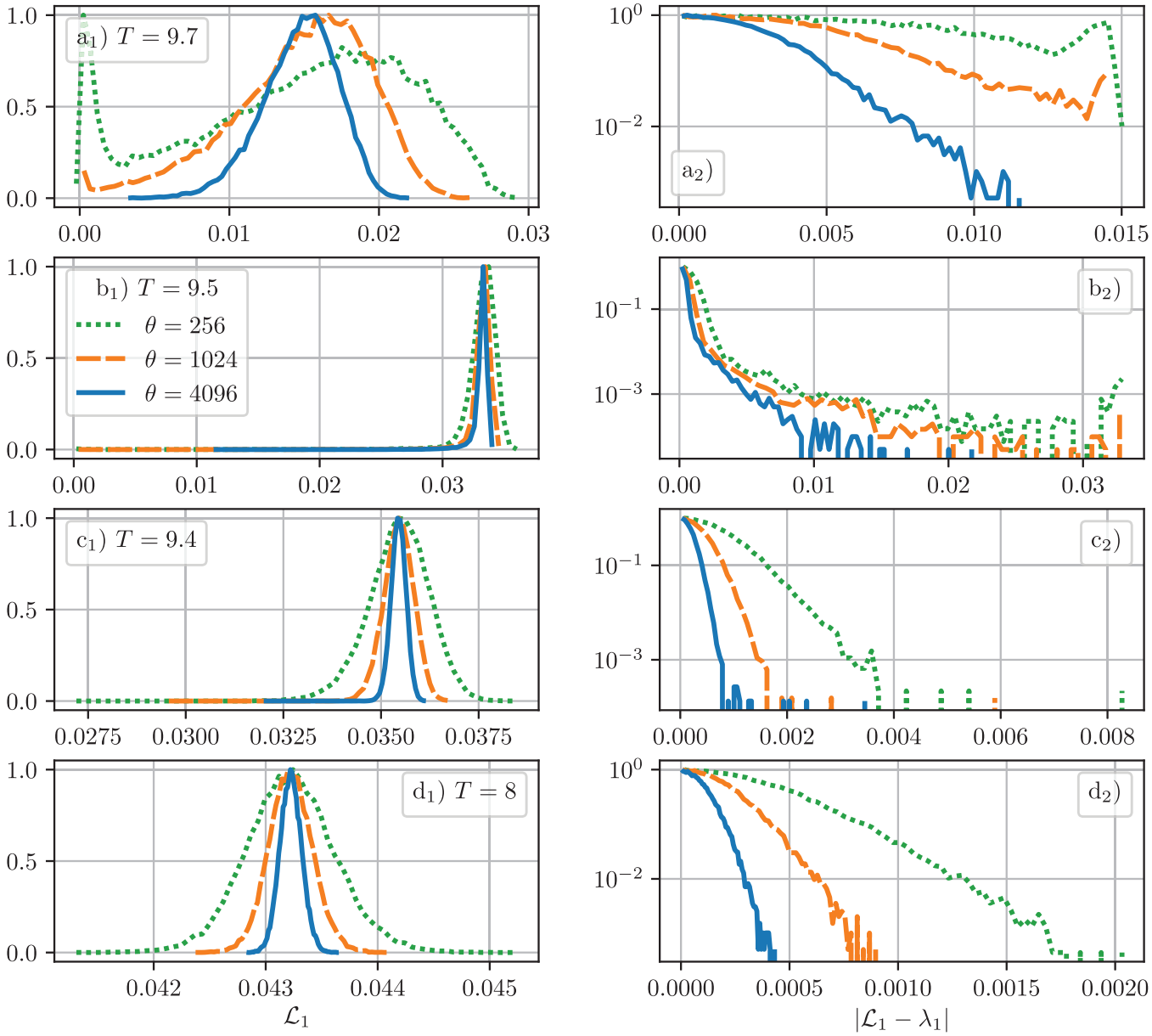

FIG. 9. PDFs of large time FTLE $\mathscr{L}_1$ computed on increasing time scales $\theta = 256$, 1024, and 4096. The log scale is used for the vertical axes in the right column.

Gaussian curves are formed because the attractor does not contain strongly competing subsets with different stability properties, and the subset responsible for the violation of the hyperbolicity has small relative weight, see Fig. 7(e).

2. Diffusion of Lyapunov exponents

Summation of FTLEs in the course of computation of Lyapunov exponents can be considered as a sort of random walking. If the summed values are random and independent, the variance of the sum is known to grow linearly in time. The coefficient of this growth, a diffusion coefficient, can be considered as one more characteristic quantifier of chaotic dynamics.[48,54] This is the case for the most of chaotic systems no matter hyperbolic or not, and it is related with the Gaussian form of PDFs of FTLEs on large times, see Figs. 9(c) and 9(d). But for non-Gaussian distributions, like the one shown in Fig. 9(b), an anomalous diffusion occurs.

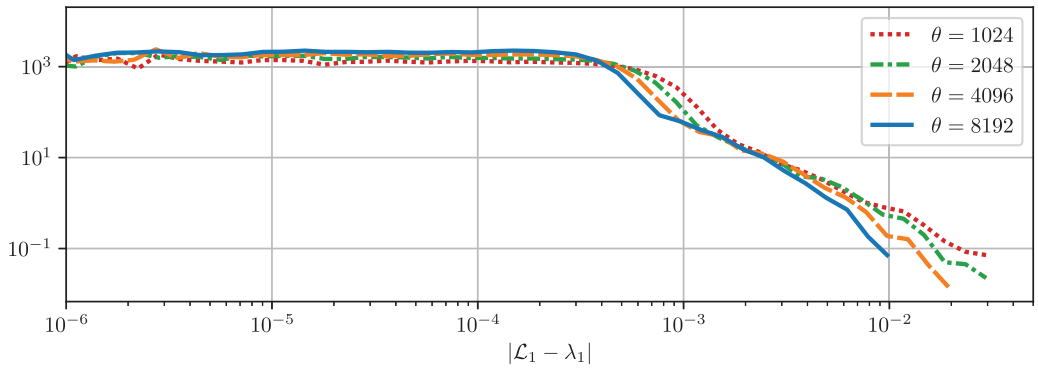

FIG. 10. PDF for deviations of $\mathcal{L}_1$ on increasing time scales for $T = 9.5$. The log–log scale is used. Observe power law decay of tails. Estimated values of the exponent α are (θ, α) = (1024, 2.24), (2048, 2.28), (4096, 3.16), and (8192, 2.72).

Let $L_i(\theta) = \mathcal{L}_i T\theta$ be a Lyapunov sum over θ steps, and let $c_{ij} = \text{Covar}[L_i(\theta), L_j(\theta)]$ be a covariance of two Lyapunov sums. To reveal anomalous diffusion, we approximate the time dependence of the covariance via a power law,

$$c_{ij} = D\theta^{\sigma}. \tag{10}$$

For a normal diffusion, $\sigma = 1$ and D is a usual diffusion coefficient. In Fig. 11, markers show c_{ij} for $i, j = 1, 2$ as functions of θ in the log–log scale. Solid lines represent computed approximations. Line for c_{12} at $T = 9.5$ in Fig. 11(c) starts beyond the origin since c_{12} for smaller θ are negative. Observe that points are very good fitted to straight lines in the log–log scale. Computed approximation at $T = 8$ are

$$c_{11} = 0.0025\,\theta^{1.00}, c_{22} = 0.0028\,\theta^{1.04}, c_{12} = 0.00093\,\theta^{0.98}, \tag{11}$$

and at $T = 9.5$ are

$$c_{11} = 0.027\,\theta^{1.27}, c_{22} = 0.044\,\theta^{1.17}, c_{12} = 0.012\,\theta^{1.31}. \tag{12}$$

We see that in area D of hyperbolic chaos at $T = 8$, the diffusion is normal: $\sigma \approx 1$. The diffusion coefficients D are of the order 10^{-3}. For a non-Gaussian case, $T = 9.5$ in area B, σ is larger than 1. It means that here we have anomalous diffusion. But, since σ is nevertheless close to 1, the comparison of D with the case at $T = 8$ makes sense yet. We see that it is of order 10^{-2}, i.e., one order higher. Altogether, it indicates much higher amplitude of fluctuations of FTLEs in the non-Gaussian case.

IV. OUTLINE AND DISCUSSION

In this paper, we have considered a nonautonomous time-delay system whose excitation parameter is periodically modulated so that the system produces a sequence of oscillation pulses. Due to a specially tuned nonlinear mechanism, the phase of the oscillations is doubled after each modulation period. As a result, a stroboscopic map for this system demonstrates hyperbolic chaos. By varying the relation between the delay time and the excitation period, one can observe a transition to regime (a) when this map operates as two weakly coupled chaotic subsystems excited alternately. The overall dynamics in this case still being hyperbolic becomes hyperchaotic with two positive Lyapunov exponents.

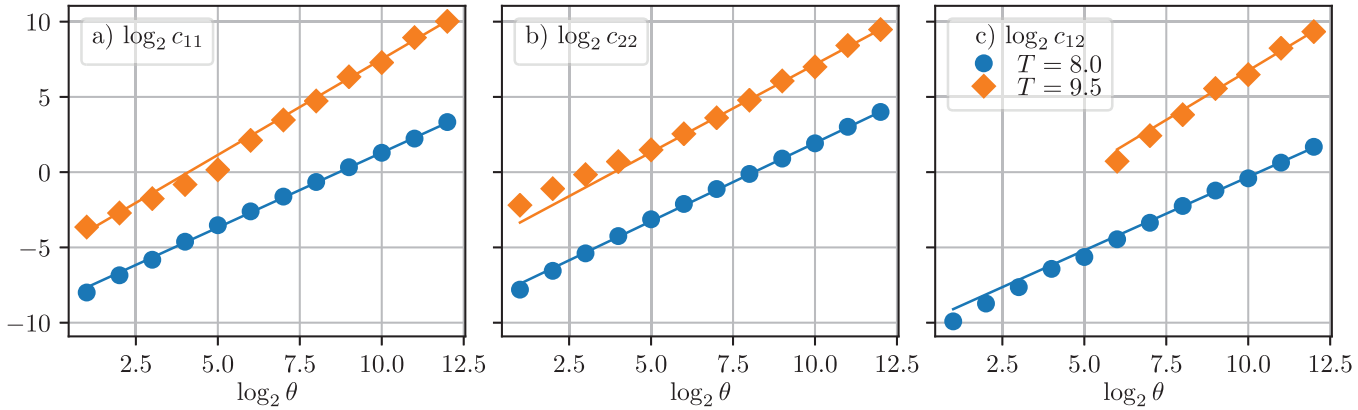

FIG. 11. Power law approximation $D\theta^{\sigma}$, see Eqs. (11) and (12) for numerical values. Only four last points are used for computing the approximations.

We have analyzed the transition to this hyperbolic hyperchaos and revealed the following scenario. After regular oscillations, the hyperchaos appears almost immediately. An area with a single positive exponent is very narrow. Then, the following hyperchaotic regimes take place sequentially: (a) intermittency as an alternation of staying near a fixed point and chaotic bursts; (b) competition between the fixed point and chaotic subset which appears near it; (c) plain hyperchaos without hyperbolicity after termination visiting neighborhoods of the fixed point; and (d) transformation of chaos to hyperbolic form.

The competition in regime (b) results in a non-Gaussian distribution of large time FTLE with power law tails and power law growth of Lyapunov sums. This type of behavior related with wandering of trajectories near subsets with different numbers of expanding directions is called unstable dimension variability (UDV). Usually, it is observed as a part of scenario of destruction of chaotic synchronization of two subsystems.[27] In our case, we also can talk about two chaotic subsystems with rather nontrivial interaction. The UDV effect is observed for them as their effective coupling strength is decreased.

The transition to hyperbolic hyperchaos (d) is accompanied by vanishing of the embedded into the attractor non-hyperbolic chaotic subset, that we have detected using covariant Lyapunov vectors. The hyperbolic hyperchaos in turn is found to be of two types. The difference is due to the presence of the degenerated hyperbolic chaotic subset. When it is visited by trajectories, the attractor gets more complicated structure with higher Kaplan–Yorke dimension, and after its vanish, the system operates just as two weakly coupled identical hyperbolic chaotic subsystems.

ACKNOWLEDGMENTS

The work of P.V.K. on theoretical formulation, elaboration of computer routines, and numerical computations was supported by a grant from the Russian Science Foundation (No. 20-71-10048).

DATA AVAILABILITY

Data sharing is not applicable to this article as no new data were created or analyzed in this study.

REFERENCES

[1]T. Kapitaniak and L. O. Chua, "Hyperchaotic attractors of unidirectionally-coupled Chua's circuits," Int. J. Bifurcation Chaos **4**, 477–482 (1994).
[2]O. Rössler, "An equation for hyperchaos," Phys. Lett. A **71**, 155–157 (1979).
[3]N. V. Stankevich, A. Dvorak, V. Astakhov, P. Jaros, M. Kapitaniak, P. Perlikowski, and T. Kapitaniak, "Chaos and hyperchaos in coupled antiphase driven Toda oscillators," Regul. Chaotic Dyn. **23**, 120–126 (2018).
[4]I. R. Garashchuk, D. I. Sinelshchikov, A. O. Kazakov, and N. A. Kudryashov, "Hyperchaos and multistability in the model of two interacting microbubble contrast agents," Chaos **29**, 063131 (2019).
[5]N. Stankevich, A. Kuznetsov, E. Popova, and E. Seleznev, "Chaos and hyperchaos via secondary Neimark–Sacker bifurcation in a model of radiophysical generator," Nonlinear Dyn. **97**, 2355–2370 (2019).
[6]S. Nikolov and S. Clodong, "Hyperchaos-chaos-hyperchaos transition in modified Rössler systems," Chaos Solitons Fractals **28**, 252–263 (2006).
[7]L. Kocarev and U. Parlitz, "General approach for chaotic synchronization with applications to communication," Phys. Rev. Lett. **74**, 5028–5031 (1995).
[8]J. H. Peng, E. J. Ding, M. Ding, and W. Yang, "Synchronizing hyperchaos with a scalar transmitted signal," Phys. Rev. Lett. **76**, 904–907 (1996).
[9]L. Yaowen, G. Guangming, Z. Hong, W. Yinghai, and G. Liang, "Synchronization of hyperchaotic harmonics in time-delay systems and its application to secure communication," Phys. Rev. E **62**, 7898–7904 (2000).
[10]J. Wang, W. Yu, J. Wang, Y. Zhao, J. Zhang, and D. Jiang, "A new six-dimensional hyperchaotic system and its secure communication circuit implementation," Int. J. Circuit Theor. Appl. **47**, 702–717 (2019).
[11]F. Sun, S. Liu, Z. Li, and Z. Lü, "A novel image encryption scheme based on spatial chaos map," Chaos Solitons Fractals **38**, 631–640 (2008).
[12]C. Zhu, "A novel image encryption scheme based on improved hyperchaotic sequences," Opt. Commun. **285**, 29–37 (2012).
[13]S. Li and X. Zheng, "Cryptanalysis of a chaotic image encryption method," in *2002 IEEE International Symposium on Circuits and Systems. Proceedings (Cat. No.02CH37353)* (IEEE, 2002), Vol. 2, p. II.
[14]R. Rhouma and S. Belghith, "Cryptanalysis of a new image encryption algorithm based on hyper-chaos," Phys. Lett. A **372**, 5973–5978 (2008).
[15]S. Torkamani, E. A. Butcher, M. D. Todd, and G. Park, "Hyperchaotic probe for damage identification using nonlinear prediction error," Mech. Syst. Signal. Process. **29**, 457–473 (2012).
[16]S. P. Kuznetsov, *Hyperbolic Chaos: A Physicist's View* (Springer-Verlag, Berlin, 2012), p. 336.
[17]S. Smale, "Differentiable dynamical systems," Bull. Am. Math. Soc. **73**, 747–817 (1967).
[18]*Dynamical Systems 9: Dynamical Systems with Hyperbolic Behaviour*, Encyclopaedia of Mathematical Sciences Vol. 9, edited by D. V. Anosov (Springer, Berlin, 1995).
[19]A. Katok and B. Hasselblatt, *Introduction to the Modern Theory of Dynamical Systems*, 1st ed., Encyclopedia of Mathematics and its Applications Vol. 54 (Cambridge University Press, 1995), p. 802.
[20]A. A. Andronov and L. S. Pontryagin, "Structurally stable systems," Dokl. Akad. Nauk SSSR **14**, 247–250.
[21]A. A. Andronov, S. E. Khaikin, and A. A. Vitt, *Theory of Oscillators* (Pergamon Press, 1966).
[22]S. P. Kuznetsov, "Dynamical chaos and uniformly hyperbolic attractors: From mathematics to physics," Phys. Usp. **54**, 119–144 (2011).
[23]P. V. Kuptsov and S. P. Kuznetsov, "Violation of hyperbolicity in a diffusive medium with local hyperbolic attractor," Phys. Rev. E **80**, 016205 (2009).
[24]P. V. Kuptsov, "Violation of hyperbolicity via unstable dimension variability in a chain with local hyperbolic chaotic attractors," J. Phys. A Math. Theor. **46**, 254016 (2013).
[25]E. J. Kostelich, I. Kan, C. Grebogi, E. Ott, and J. A. Yorke, "Unstable dimension variability: A source of nonhyperbolicity in chaotic systems," Physica D **109**, 81–90 (1997), Proceedings of the Workshop on Physics and Dynamics between Chaos, Order, and Noise.
[26]R. F. Pereira, S. E. de S. Pinto, R. L. Viana, S. R. Lopes, and C. Grebogi, "Periodic orbit analysis at the onset of the unstable dimension variability and at the blowout bifurcation," Chaos **17**, 023131 (2007).
[27]T. Kapitaniak, Y. Maistrenko, and S. Popovych, "Chaos-hyperchaos transition," Phys. Rev. E **62**, 1972–1976 (2000).
[28]S. Yanchuk and T. Kapitaniak, "Chaos-hyperchaos transition in coupled Rössler systems," Phys. Lett. A **290**, 139–144 (2001).
[29]S. Yanchuk and T. Kapitaniak, "Symmetry-increasing bifurcation as a predictor of a chaos-hyperchaos transition in coupled systems," Phys. Rev. E **64**, 056235 (2001).
[30]*Delay Systems: From Theory to Numerics and Applications*, edited by T. Vyhlídal, J. F. Lafay, and R. Sipahi (Springer Science & Business Media, 2013), Vol. 1.
[31]S. P. Kuznetsov and V. I. Ponomarenko, "Realization of a strange attractor of the Smale-Williams type in a radiotechnical delay-feedback oscillator," Tech. Phys. Lett. **34**, 771–773 (2008).
[32]S. P. Kuznetsov and A. Pikovsky, "Attractor of Smale-Williams type in an autonomous time-delay system," arXiv:1011.5972 (2010).
[33]S. P. Kuznetsov and A. Pikovsky, "Hyperbolic chaos in the phase dynamics of a Q-switched oscillator with delayed nonlinear feedbacks," Europhys. Lett. **84**, 10013 (2008).

[34]S. V. Baranov, S. P. Kuznetsov, and V. I. Ponomarenko, "Chaos in the phase dynamics of Q-switched van der Pol oscillator with additional delayed-feedback loop," Izvestiya VUZ. Appl. Nonlinear Dyn. **18**, 12–23 (2010) (in Russian).
[35]A. S. Kuznetsov and S. P. Kuznetsov, "Parametric generation of robust chaos with time-delayed feedback and modulated pump source," Commun. Nonlinear Sci. Numer. Simul. **18**, 728–734 (2013).
[36]D. S. Arzhanukhina and S. P. Kuznetsov, "Robust chaos in autonomous time-delay system," Izvestiya VUZ. Appl. Nonlinear Dyn. **22**, 36–49 (2014); arxiv:1404.4221 (in Russian).
[37]P. V. Kuptsov and S. P. Kuznetsov, "Numerical test for hyperbolicity of chaotic dynamics in time-delay systems," Phys. Rev. E **94**, 010201(R) (2016).
[38]P. V. Kuptsov and S. P. Kuznetsov, "Numerical test for hyperbolicity in chaotic systems with multiple time delays," Commun. Nonlinear Sci. Numer. Simul. **56**, 227–239 (2018).
[39]S. V. Baranov and S. P. Kuznetsov, "Hyperchaos in a system with delayed feedback loop based on Q-switched van der Pol oscillator," Izvestiya VUZ. Appl. Nonlinear Dyn. **18**, 111–120 (2010) (in Russian).
[40]S. P. Kuznetsov, "Example of a physical system with a hyperbolic attractor of the Smale-Williams type," Phys. Rev. Lett. **95**, 144101 (2005).
[41]F. Ginelli, P. Poggi, A. Turchi, H. Chaté, R. Livi, and A. Politi, "Characterizing dynamics with covariant Lyapunov vectors," Phys. Rev. Lett. **99**, 130601 (2007).
[42]C. L. Wolfe and R. M. Samelson, "An efficient method for recovering Lyapunov vectors from singular vectors," Tellus A Dyn. Meteorol. Oceanogr. **59**, 355–366 (2007).
[43]P. V. Kuptsov and U. Parlitz, "Theory and computation of covariant Lyapunov vectors," J. Nonlinear. Sci. **22**, 727–762 (2012).
[44]A. Pikovsky and A. Politi, *Lyapunov Exponents: A Tool to Explore Complex Dynamics* (Cambridge University Press, 2016), p. 295.
[45]J. L. Kaplan and J. A. Yorke, "Chaotic behavior of multidimensional difference equations," in *Functional Differential Equations and Approximations of Fixed Points*, Lecture Notes in Mathematics Vol. 730, edited by H.-O. Peitgen and H.-O. Walter (Springer, Berlin, 1979), p. 204.
[46]P. Grassberger and I. Procaccia, "Measuring the strangeness of strange attractors," Physica D **9**, 189–208 (1983).
[47]P. V. Kuptsov and S. P. Kuznetsov, "Lyapunov analysis of strange pseudohyperbolic attractors: Angles between tangent subspaces, local volume expansion and contraction," Regul. Chaotic Dyn. **23**, 908–932 (2018).
[48]P. V. Kuptsov and A. Politi, "Large-deviation approach to space-time chaos," Phys. Rev. Lett. **107**, 114101 (2011).
[49]P. V. Kuptsov, "Fast numerical test of hyperbolic chaos," Phys. Rev. E **85**, 015203 (2012).
[50]R. L. Davidchack and Y.-C. Lai, "Efficient algorithm for detecting unstable periodic orbits in chaotic systems," Phys. Rev. E **60**, 6172–6175 (1999).
[51]J. Crofts and R. Davidchack, "Efficient detection of periodic orbits in chaotic systems by stabilizing transformations," SIAM J. Sci. Comput. **28**, 1275–1288 (2006).
[52]J. J. Crofts and R. L. Davidchack, "On the use of stabilizing transformations for detecting unstable periodic orbits in high-dimensional flows," Chaos **19**, 033138 (2009).
[53]J. Alstott, E. Bullmore, and D. Plenz, "Powerlaw: A python package for analysis of heavy-tailed distributions," PLoS ONE **9**, 1–11 (2014).
[54]H. Fujisaka, "Statistical dynamics generated by fluctuations of local Lyapunov exponents," Prog. Theor. Phys. **70**, 1264–1275 (1983).